FOUNDATIONS
ADVANCES

ISSN: 2053-2733
journals.iucr.org/a

Experimental and theoretical investigations of an X-ray LLL interferometer with a wedge-shaped mirror plate

Tigran H. Eyramjyan, Tamara S. Mnatsakanyan and Minas K. Balyan

Acta Cryst. (2018). A**74**, 595–599

Acta Cryst A FOUNDATIONS ADVANCES
ISSN 2053-2733

Experimental and theoretical investigations of an X-ray LLL interferometer with a wedge-shaped mirror plate

Tigran H. Eyramjyan,* Tamara S. Mnatsakanyan and Minas K. Balyan

Faculty of Physics, Chair of Solid State Physics, Yerevan State University, 1 Alex Manoogian, Yerevan 0025, Armenia. *Correspondence e-mail: tigeyro@ysu.am

Received 9 February 2018
Accepted 10 July 2018

Edited by K. Tsuda, Tohoku University, Japan

Keywords: LLL interferometers; wedge-shaped mirror plate; *Pendellösung* fringes; Moiré fringes; superposition.

An X-ray LLL interferometer with a wedge-shaped mirror plate is experimentally and theoretically investigated. Experimentally obtained interference patterns show that the Moiré fringes are superposed on *Pendellösung* fringes and the period of the *Pendellösung* fringes is not changed after passing the analyzer plate. An eikonal theory of interference-fringe formation in an LLL interferometer with a wedge-shaped mirror plate is developed, and provides predictions that coincide with experimentally obtained results.

1. Introduction

The well known LLL X-ray interferometer was proposed by Bonse & Hart (1965*a*,*b*). The interferometer consists of three crystalline plates with an almost perfect structure. An X-ray beam falls on the first splitter plate (S) at the exact Bragg angle and is divided into transmitted and diffracted beams. These beams fall on the second mirror (M) plate. The mirror plate forms two beams that interfere in the third analyzer plate (A). At the exit surface of the third plate, interference fringes are formed between two beams, which are called Moiré fringes. Since in all plates Laue-case diffraction occurs, this type of interferometer is called an LLL interferometer. Interferometers BBB with three Bragg-case reflections (Bonse & Hart, 1966) and based on three-beam diffraction (Graeff & Bonse, 1977) have also been suggested. Interferometers of the types LBL, LBBL and BLB with mixed Laue- and Bragg-case diffractions were suggested in the article by Bonse & Hart (1968). An LLLL interferometer with four plates was suggested and tested by Eyramdjyan *et al.* (1973). An LLL interferometer with a stepped mirror block was investigated by Gasparyan *et al.* (1991). The edge of the step is perpendicular to the plane of diffraction. The Hart–Milne interferometer (Hart & Milne, 1968) consists of a wedge-shaped thin plate and a thick crystalline plate. In this interferometer, *Pendellösung* fringes or fringes of constant thickness are formed. For references of applications of X-ray interferometers see Authier (2001) and Pinsker (1982). In the work by Alumyan & Eyramdjyan (2005), an LLL interferometer with a wedge-shaped mirror plate was suggested and experimentally investigated, in which the mirror plate and the analyzer plate form the Hart–Milne interferometer. Thus, this interferometer is a combination of the Hart–Milne interferometer and an LLL interferometer. The section interference patterns obtained in this interferometer show that the *Pendellösung* fringes are superposed on the Moiré pattern. In this work, a theoretical explanation of the obtained result was

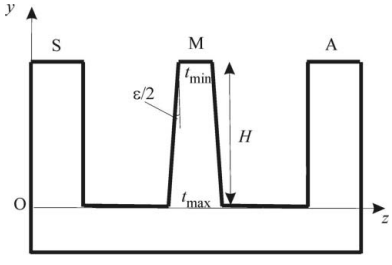

not given. In the work by Balyan & Gabrielyan (1994) and Balyan (2012), an eikonal theory of X-ray Moiré-pattern formation in an LLL interferometer was described. Balyan & Gabrielyan (1994) made the assumption that weak deformations exist only in the analyzer plate; however, Balyan (2012) assumed that weak deformations exist in all plates of the interferometer. This theory has been applied to the case with a constant temperature gradient in the mirror plate of the interferometer (Balyan, 2017).

In this work, the theory given by Balyan (2012) is improved for the case where the mirror plate is wedge shaped. This theory is applied to the explanation of the superposition of the *Pendellösung* fringes on the Moiré pattern in the interferometer suggested by Alumyan & Eyramdjyan (2005). The *Pendellösung* and Moiré fringes in such an interferometer are experimentally investigated. The theory explains the obtained interference patterns and the experiment confirms the theoretically obtained results.

2. Experimental

The scheme of an LLL interferometer is shown in Fig. 1(*a*). Our experiments were performed using an interferometer of the same type but with a wedge-shaped mirror plate (Fig. 1*b*). The interferometer is fabricated for Mo $K\alpha_1$ radiation and for Si(220) symmetrical Laue-case reflections using a dislocation-free silicon crystal. The thicknesses of the splitter plate and the

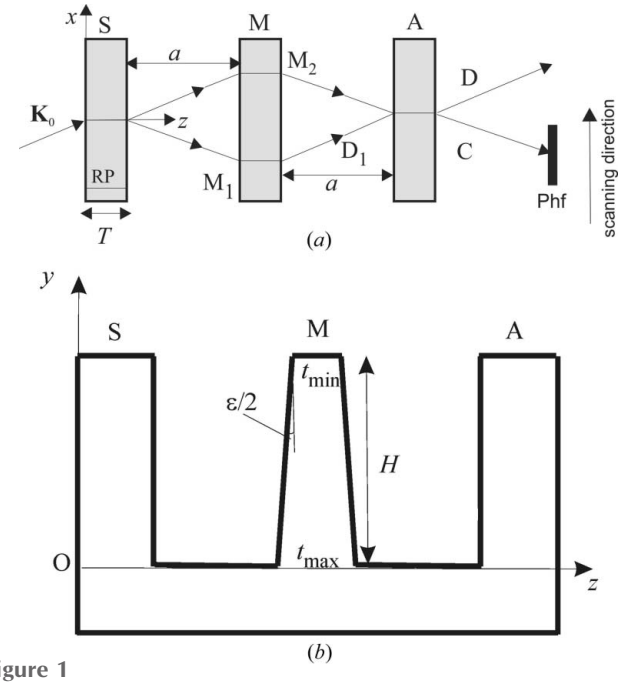

Figure 1
(*a*) X-ray three-plate interferometer, top view. $\mathbf{K}_0$ is the wavevector of the incident wave, RP refers to the reflecting planes, T is the thickness of the plates, x and z are coordinates, S is the splitter, M is the mirror plate (with M_1 and M_2 regions), A is the analyzer plate, a is the distance between the plates, D_1 is the double diffracted beam, C and D are emerging from the interferometer beams, and Phf is the photographic film; the simultaneous scanning direction of the interferometer and the photographic film is shown. (*b*) X-ray three-plate interferometer with wedge-shaped mirror plate. Side view.

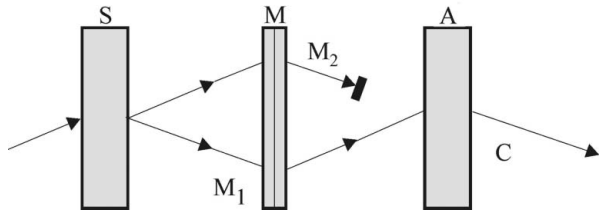

Figure 2
Ray trajectories in the interferometer with stopped beam after the wedge-shaped mirror plate.

analyzer plate are $T = 3.4$ mm and $\mu T \simeq 5$, respectively, where $\mu = 1.42$ mm^{-1} is the linear absorption coefficient for silicon. Through these plates only weakly absorbing σ-polarization modes can pass. The maximum thickness of the wedge at the base of the interferometer is $t_{max} = 0.8$ mm and the minimal thickness of the wedge is $t_{min} = 0.2$ mm. The height of the plates is $H = 16.2$ mm (Fig. 1*b*). The angle of the wedge is determined from the expression

$$\varepsilon \simeq 2\tan\frac{\varepsilon}{2} = \frac{t_{max} - t_{min}}{H}, \qquad (1)$$

and its numerical value in our case is 2.1°. For the wedge-shaped plate, $\mu t_{min} \simeq 0.3$ and $\mu t_{max} \simeq 1.14$. The two modes of the dispersion surface can pass through this plate.

First we had the usual LLL interferometer (Fig. 1*a*) with inherent Moiré fringes. Then by chemical and mechanical processing, the mirror plate was reformed to the wedge-shaped form, keeping the ideal geometry of the interferometer (Fig. 1*b*).

An X-ray laboratory source was used for the structural analysis. The size of the source was 0.4 mm in the diffraction plane. The length of the collimator of the X-ray chamber is 0.4 m and the width of the beam incident on the interferometer in the diffraction plane was 0.3 mm. The experiments were performed at 40 kV and 20 mA. The interference patterns are recorded in the beams D_1, C and D by using photographic films which were placed after the wedge-shaped plate and the analyzer plate (Fig. 1*a*). If one of the beams after the wedge-shaped plate is stopped (Fig. 2), then the mirror plate and the analyzer plate will form a Hart–Milne interferometer (Hart & Milne, 1968) and the splitter has the role of a monochromator.

In Figs. 3(*a*) and 3(*b*), the interference patterns (*Pendellösung* fringes) in the doubly diffracted beam D_1 and in the triply diffracted beam C are shown. If the beam after the mirror plate is not stopped, then fringes of constant thickness (*Pendellösung* fringes) with quasi-monochromatic radiation in the doubly diffracted beam D_1 are obtained (Fig. 4*a*). In the triply diffracted beam C, the interference pattern is the superposition of the *Pendellösung* and Moiré fringes (Fig. 4*b*). The same pattern will be obtained in beam D. The dimensions in Figs. 4(*a*) and 4(*b*) are approximately the same as in Fig. 3.

It must be noted that the interference pattern in Fig. 3(*b*) differs from the interference pattern in Fig. 4(*b*). Since in Fig. 4 the interference region is small, the superposition of the Moiré and *Pendellösung* fringes can hardly be seen. To reveal the

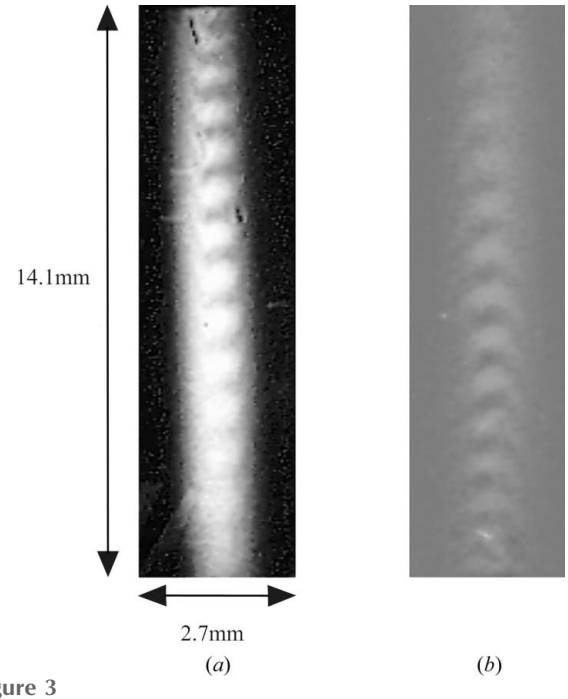

Figure 3
The beam emerging from region M_2 of the mirror plate is stopped. The dimensions are 14.1 mm (height) and 2.7 mm (width). *Pendellösung* fringes (*a*) in the doubly diffracted beam D_1 and (*b*) in the triply diffracted beam C.

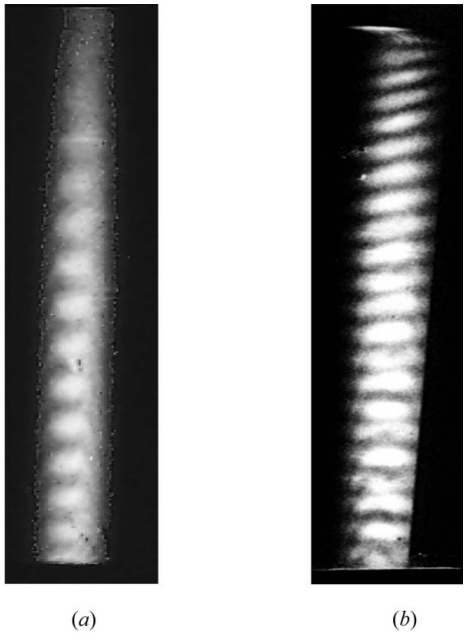

Figure 4
No stopped beam. (*a*) *Pendellösung* fringes in the doubly diffracted beam D_1. (*b*) superposed *Pendellösung* and Moiré fringes in the triply diffracted beam C.

superposition, the interference region was increased by simultaneous scanning of the interferometer and the photographic film.

The region of interference patterns increases and the superposition of the *Pendellösung* and Moiré fringes is revealed (Figs. 5*a* and 5*b*). In Fig. 5(*a*) the interference pattern

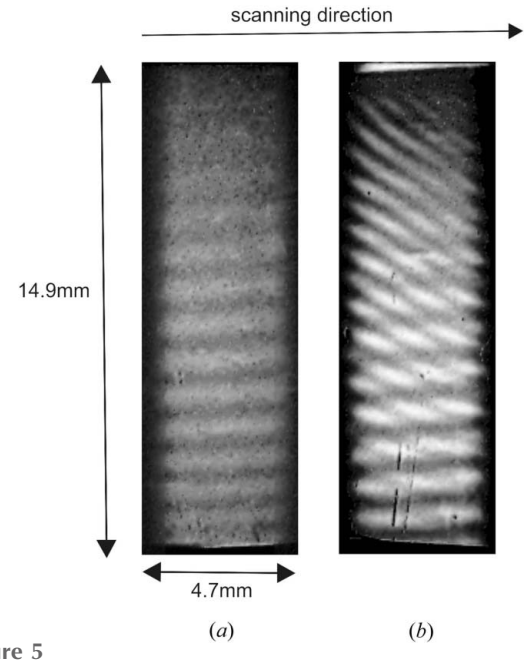

Figure 5
The interference patterns when scanning the interferometer and the photographic film simultaneously. (*a*) *Pendellösung* fringes in the doubly diffracted beam D_1. (*b*) Superposition of the *Pendellösung* fringes and the Moiré fringes in the triply diffracted beam C. The simultaneous scanning direction of the interferometer and the photographic film is shown.

(*Pendellösung* fringes) in the doubly diffracted beam D_1 is shown; these are the plane-wave *Pendellösung* fringes. In Fig. 5(*b*), the interference pattern in beam C is shown and the superposition of the *Pendellösung* and Moiré fringes can be clearly seen.

3. Theory

In this section, we briefly describe the derivation of the Moiré fringes' intensity-distribution formula, using the eikonal theory for weakly deformed crystals. The incident plane wave case is considered. The detailed theory for usual interferometers has been given by Balyan & Gabrielyan (1994) and Balyan (2012). In this article, the mirror plate is considered to be wedge shaped. The relevant theory must take into account the fact that the two modes of the σ-polarization pass through the mirror plate. The other two plates of the interferometer satisfy the condition $\mu T \gg 1$ and only the weakly absorbing modes can pass through these plates. It is assumed that weak deformations exist in all plates of the interferometer. It is also assumed that the deformations slowly vary over distances of the order of the extinction length,

$$\left|\frac{\partial^2 \mathbf{hu}}{\partial s_0 \partial s_h}\right| \ll |\sigma^2|, \qquad (2)$$

where $\mathbf{h}$ is the diffraction vector, s_0 and s_h are the oblique coordinates along the propagation directions of the transmitted and the diffracted waves, $\mathbf{u}$ is the displacement vector of the atoms from their equilibrium positions in the perfect crystal, $\sigma^2 = k^2\chi_h\chi_{\bar{h}}/4$, χ_h and $\chi_{\bar{h}}$ are the Fourier coefficients of

the susceptibility of the crystal for the diffraction vector **h**, and $k = 2\pi/\lambda$ is the wavenumber. The inequality (2) is the condition of the eikonal approximation. Moreover, it is assumed that the deformations are weak,

$$|\alpha| \ll |\chi_h|, \tag{3}$$

where $\alpha = -(2/k)\partial\mathbf{hu}/\partial s_h$ is the local deviation parameter from the Bragg exact condition. The physical sense of inequality (3) is that deformations do not deflect the directions of the waves beyond the limits of the reflection curve. If inequalities (2) and (3) are fulfilled, the eikonal theory for weakly deformed crystals can be applied (Indenbom & Chukovskii, 1972; Balyan, 2012). The amplitudes of the transmitted and diffracted waves have the forms $E_0\exp(i\Phi)$ and $E_h\exp[i(\Phi-\mathbf{hu})]$, respectively, where Φ is the eikonal. In the case of the incident plane wave at the exact Bragg angle, the eikonal in the weakly deformed crystal is chosen to have the form $\Phi^{(1),(2)} = \pm\sigma z/\cos\theta$, where 1 and 2 denote the two branches of the dispersion surface and the sign '+' corresponds to the weakly absorbing mode 1. In this case, the transport equations of the amplitudes have the form

$$\begin{aligned} \partial E_0/\partial z + i\frac{k\alpha}{4\cos\theta}E_0 = 0,\\ \partial E_h/\partial z + i\frac{k\alpha}{4\cos\theta}E_h = 0. \end{aligned} \tag{4}$$

The solution of equation (4) is

$$E_{0,h} = f_{0,h}\exp\left[-i\frac{k}{4\cos\theta}\int_{z_1}^{z}\alpha\,\mathrm{d}z'\right], \tag{5}$$

where $f_{0,h}$ are independent of z and the values of the amplitudes are given at $z = z_1$. After applying equation (5) in the case of the usual LLL interferometer, the following expressions for the intensity distribution in beams C and D were found (Balyan, 2012):

$$I = \frac{E_0^{(i)2}}{32}\exp\left[-\frac{3\mu T}{\cos\theta}\left(1-\frac{\chi_{hi}}{\chi_{0i}}\right)\right](1+\cos\beta), \tag{6}$$

where χ_{0i} and χ_{hi} are zero-order and **h**-order Fourier coefficients of the imaginary part of the crystal susceptibility, $\mu = \chi_{0i}$ is the linear absorption coefficient of the crystal, β is the phase difference of the interfering beams at the exit surface of the analyzer plate, where

$$\begin{aligned} \beta(x,y) = &-\mathbf{hu}_1^{\mathrm{e}} + \frac{1}{2}[\mathbf{hu}_2^{\mathrm{i}}(x - a\tan\theta) + \mathbf{hu}_2^{\mathrm{e}}(x - a\tan\theta)]\\ &+\frac{1}{2}[\mathbf{hu}_3^{\mathrm{i}}(x + a\tan\theta) + \mathbf{hu}_3^{\mathrm{e}}(x + a\tan\theta)] - \mathbf{hu}_4^{\mathrm{i}}\\ &-\frac{1}{2}\tan\theta\frac{\partial}{\partial x}\int_{T+a}^{2T+a}\mathbf{hu}_2\,\mathrm{d}z'|_{x\to x-a\tan\theta}\\ &+\frac{1}{2}\tan\theta\frac{\partial}{\partial x}\int_{T+a}^{2T+a}\mathbf{hu}_3\,\mathrm{d}z'|_{x\to x+a\tan\theta}, \end{aligned} \tag{7}$$

$\mathbf{u}_1$ is the displacement vector in the splitter, $\mathbf{u}_2$ and $\mathbf{u}_3$ are the displacement vectors in the regions M_1 and M_2 of the mirror plate, and $\mathbf{u}_4$ is the displacement vector in the analyzer. The upper indices of the displacement vectors 'i' and 'e' mean the entrance surface and the exit surface of the corresponding plate. The diffraction absorption coefficient is written for the centrosymmetric crystal since, for most cases, centrosymmetric crystals are used in the interferometers.

Applying the eikonal theory for weakly deformed crystals for an LLL interferometer with a wedge-shaped mirror plate, and repeating the derivations, instead of equations (6) and (7), one obtains

$$\begin{aligned} I = &\frac{E_0^{(i)2}}{8}\exp\left[-\frac{\mu t(y)}{\cos\theta}\right]\exp\left[-\frac{2\mu T}{\cos\theta}\left(1-\frac{\chi_{hi}}{\chi_{0i}}\right)\right],\\ &\times\left|\sin\left[\frac{\pi t(y)}{\Lambda}\right]\right|^2(1+\cos\beta) \end{aligned} \tag{8}$$

and

$$\begin{aligned} \beta(x,y) = &-\mathbf{hu}_1^{\mathrm{e}} + \frac{1}{2}[\mathbf{hu}_2^{\mathrm{i}}(x - a\tan\theta) + \mathbf{hu}_2^{\mathrm{e}}(x - a\tan\theta)]\\ &+\frac{1}{2}[\mathbf{hu}_3^{\mathrm{i}}(x + a\tan\theta) + \mathbf{hu}_3^{\mathrm{e}}(x + a\tan\theta)] - \mathbf{hu}_4^{\mathrm{i}}\\ &-\frac{1}{2}\tan\theta\frac{\partial}{\partial x}\int_{T+a}^{T+t(y)+a}\mathbf{hu}_2\,\mathrm{d}z'|_{x\to x-a\tan\theta} + \frac{1}{2}\tan\theta\frac{\partial}{\partial x}\\ &\times\int_{T+a}^{T+t(y)+a}\mathbf{hu}_3\,\mathrm{d}z'|_{x\to x+a\tan\theta}, \end{aligned} \tag{9}$$

where $\lambda = \lambda\cos\theta/(\chi_h\chi_{\bar{h}})^{1/2}$ ($\Lambda_r = \mathrm{Re}\Lambda = \lambda\cos\theta/|\chi_{hr}|$ is the extinction length), $t(y)$ is the thickness of the mirror plate and is a function of the y coordinate, and the axis Oy is vertically oriented from the base of the interferometer (Fig. 1*b*):

$$t(y) = \frac{t_{\min} - t_{\max}}{H}y + t_{\max} = -\varepsilon y + t_{\max}. \tag{10}$$

It should be noted that the distance between the plates (a) is also a function of the y coordinate.

4. Discussion

From equation (8), it is seen that the intensity of the *Pendellösung* fringes is proportional to $|\sin[\pi t(y)/\Lambda]|^2$ and the intensity of the Moiré fringes is proportional to $1 + \cos\beta$. Therefore, these two sets of the interference fringes are superposed and the maxima of the resulting interference patterns are the intersection points of the maxima of these two sets of interference fringes. The period after the mirror plate of the *Pendellösung* fringes will be

$$L = \Lambda_r\frac{H}{t_{\max} - t_{\min}} = \frac{\Lambda_r}{\varepsilon}, \tag{11}$$

which in our case is about 1 mm. According to equation (8), the period of these fringes must also be the same after the

analyzer plate in both the C and D beams. The *Pendellösung* fringes are not displaced after passing the analyzer plate.

To examine these predictions derived from the theory, let us refer to the interference patterns in Figs. 5(*a*) and 5(*b*). According to Fig. 5(*b*), the *Pendellösung* fringes are really superposed with the Moiré fringes, and the intersection points of these two sets of fringes have maximum intensity. The *Pendellösung* fringes are not displaced with respect to their positions after the second plate. The period of the *Pendellösung* fringes was measured after the second (Fig. 5*a*) and the third (Fig. 5*b*) plate of the interferometer. In both cases the approximate value of 1 mm was obtained, which coincides with theoretically obtained value according to equation (11). Therefore, the conclusion that the period of the *Pendellösung* fringes is the same after the second and third plates of the interferometer has also been verified. So theory and experiment give consistent results.

5. Summary

The LLL interferometer with a wedge-shaped mirror plate suggested by Alumyan & Eyramdjyan (2005) has been experimentally and theoretically investigated. The experimentally obtained interference patterns after the mirror and analyzer plates show that the *Pendellösung* fringes are superposed with the Moiré fringes, the *Pendellösung* fringes are not displaced and the period of these fringes is the same after the second and third plates of the interferometer. An eikonal theory of interference-fringe formation in the suggested interferometer with a wedge-shaped mirror plate is developed for the case of an incident plane wave. According to this theory, these two sets of interference fringes should be superposed, the maximal intensity must be at the intersection points of these two sets of fringes, the *Pendellösung* fringes must not be displaced and the *Pendellösung*-fringe period must be the same after the second and third plates of the interferometer. The measurements performed show a satisfactory consistency between theory and experiment.

References

Alumyan, K. V. & Eyramdjyan, T. O. (2005). *Uchenie Zap. EGU, Estestv. Nauk.* **206**, 136–137.

Authier, A. (2001). *Dynamical Theory of X-ray Diffraction.* Oxford University Press.

Balyan, M. K. (2012). *J. Contemp. Phys.* **47**, 241–247.

Balyan, M. K. (2017). *J. Contemp. Phys.* **52**, 220–226.

Balyan, M. K. & Gabrielyan, K. T. (1994). *Proc. Natl Acad. Sci. Armen. Phys.* **29**, 118–125.

Bonse, U. & Hart, M. (1965*a*). *Appl. Phys. Lett.* **6**, 155–156.

Bonse, U. & Hart, M. (1965*b*). *Appl. Phys. Lett.* **7**, 99–100.

Bonse, U. & Hart, M. (1966). *Z. Phys.* **194**, 1–17.

Bonse, U. & Hart, M. (1968). *Acta Cryst.* A**24**, 240–245.

Eyramdjyan, F. O., Trouni, K. G. & Bezirganyan, P. H. (1973). *Proc. Natl Acad. Sci. Armen. Phys.* **8**, 193–196.

Gasparyan, L. G., Bezirganyan, P. H., Mkrtchyan, V. P., Trouni, K. G. & Toneyan, A. G. (1991). *Phys. Status Solidi A*, **123**, 77–82.

Graeff, W. & Bonse, U. (1977). *Z. Phys. B*, **27**, 19–32.

Hart, M. & Milne, A. D. (1968). *Phys. Status Solidi B*, **26**, 185–189.

Indenbom, V. & Chukhovskii, F. N. (1972). *Sov. Phys. Usp.* **15**, 298–317.

Pinsker, Z. G. (1982). *X-ray Crystallooptics.* Moscow: Nauka.